

# Microfluidic counterflow centrifugal elutriation system for sedimentation-based cell separation

Tomoki Morijiri · Masumi Yamada ·  
Toshikatsu Hikida · Minoru Seki

Received: 5 January 2012 / Accepted: 11 April 2012 / Published online: 30 November 2012  
© Springer-Verlag Berlin Heidelberg 2012

**Abstract** We present a centrifugal microfluidic system for precise cell/particle sorting using the concept of counterflow centrifugal elutriation (CCE). A conventional CCE system uses a rotor device incorporating a flow-through separation chamber, in which the balance of centrifugal and counterflow drag forces exerted on particles is gradually shifted by changing the flow rate and/or the rotation speed. In the present system, both the centrifugal and the fluid forces are generated through microdevice rotation in order to significantly simplify the setup of the conventional CCE. In addition, the density gradient of the medium is employed to elute particles/cells of different sedimentation velocities stepwise from the separation chamber instead of changing the rotation speed. We successfully separated polymer particles with diameters of 1.0–5.0  $\mu\text{m}$  using a branched loading channel for focusing particles to the center of the separation chamber. We also demonstrated the sorting of blood cells for biological applications. This system may provide a versatile means for cell/particle sorting in a general biological laboratory and function as a unit operation in various centrifugal microfluidic platforms for biochemical experiments and clinical diagnosis.

**Keywords** Centrifugal microfluidics · Cell separation · Elutriation · Sedimentation

## 1 Introduction

Cell separation is one of the most important applications of microfluidic technologies, because microchannel structures are suitable for manipulating biological particulates with sizes similar to the microchannel dimensions. Various types of microfluidic cell sorters have been developed that have achieved continuous cell separation using a stable laminar flow profile formed inside microchannels (Pamme 2007). Various physicochemical properties of cells were used to separate cells, such as size (Yamada and Seki 2005; Davis et al. 2006), density (Huh et al. 2007; Morijiri et al. 2011), surface markers (Nagrath et al. 2007), deformability (Hou et al. 2010), and shape (Sugaya et al. 2011). These microfluidic cell sorters enable highly accurate cell separation in many applications, from blood cell sorting to selective enrichment/removal of stem cells or cancer cells, using relatively simple experimental operations. However, most of these techniques require the simultaneous introduction of multiple fluids with and without cells, and so outer pressure-driven pumping devices are needed. Pumping devices can hinder the wide availability of microfluidic cell sorters for general biological experiments and their integration into a compact setup.

Centrifugal pumping systems have recently drawn great attention as a means for driving fluids in integrated bioassay systems. In centrifugal microfluidics, the artificial gravity field intrinsically drives a pumping force without actuation apart from a rotary drive (Ducrée et al. 2007; Gorkin et al. 2010), suitable for operating multiple fluids in parallel. In addition, one can accurately control the pumping speed by precisely adjusting the rotary drive rotation speed. Moreover, rotation equipment such as a centrifugal device is commonly used in biological laboratories, which can be adopted for centrifugal microdevices. Due to these

T. Morijiri · M. Yamada · T. Hikida · M. Seki (✉)  
Department of Applied Chemistry and Biotechnology,  
Graduate School of Engineering, Chiba University,  
1-33 Yayoi-cho, Inage-ku, Chiba 263-8522, Japan  
e-mail: mseki@faculty.chiba-u.jp

advantages, researchers have not only developed various types of microfluidic components for fluid manipulation, such as batch mode fluid mixing (Grumann et al. 2005), fluid switching (Kim et al. 2008), and active or passive valves (Duffy et al. 1999; Brenner et al. 2005; Kim et al. 2008; Gorkin et al. 2012), but have also proposed integrated chemical/biological analysis systems utilizing centrifugal microfluidics (Duffy et al. 1999; Steigert et al. 2006; Cho et al. 2007; Lee et al. 2009; Siegrist et al. 2010). However, cell-sorting systems based on centrifugal microfluidics have only been reported for blood separation into plasma and cells (Haerberle et al. 2006) and density-based particle sorting (Morijiri et al. 2011). A robust system for cell sorting into multiple fractions using centrifugal microfluidics would facilitate their wider usage for biological experiments and clinical diagnosis. In addition, such a system would be beneficial as a unit operation for integrated microfluidic devices driven by centrifugal manipulations.

Counterflow centrifugal elutriation (CCE) is a versatile technique for sorting cells into multiple fractions based on sedimentation velocity (Bauer 1999). In a CCE system, a buffer flow is continuously pumped through a channel systems integrated with a 3D cone-shaped flow-through separation chamber rotating as a part of a rotor in a centrifuge. Once a cell suspension is injected into the channel system, cells are loaded into the rotating separation chamber and then subjected to the centrifugal force in an outward direction and to the fluid force in an inward direction. The cone-shaped geometry of the separation chamber generates a gradient in the fluid force and therefore larger- and/or higher-density cells are retained in a narrower region of the chamber with a relatively high flow speed, where the centrifugal and fluidic forces are balanced. In contrast, smaller- and/or lower-density cells are retained in the wider region. Gradually changing the balance between the centrifugal and fluid forces by changing pumping flow rate and/or rotation speed enables the stepwise elution of the cells mainly based on size and density. CCE systems have widely been used in biological experiments, such as the separation of blood cells (Wahl et al. 1984; Faradji et al. 1994; Gibbs et al. 2008), isolation of stem or progenitor cells (Uchida and Weissman 1992; Overturf et al. 1999), and synchronization of cell cycles (Donaldson et al. 1997). Although a conventional CCE system requires expensive and highly complicated instruments such as a flow-through channel-integrated rotor and a flow rate-adjustable pump, it is a powerful technique for achieving precise cell separation into multiple fractions.

In this study, we present a microfluidic cell-sorting system that enables sedimentation velocity-based cell separation by implementing the mechanism of CCE, but with a much simpler experimental setup and operation. The most remarkable advantage of the present system is that

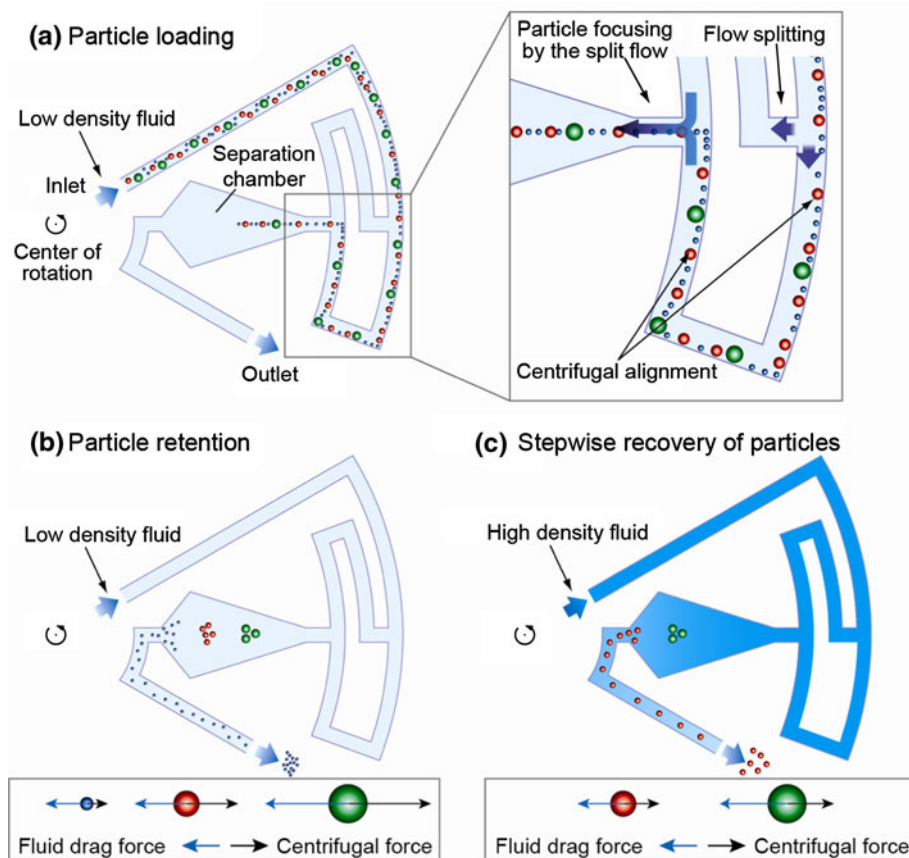
both the centrifugal force and the fluid flow are generated by microdevice rotation, and so a flow channel-integrated rotor system is not required as in a conventional CCE. In addition, in order to gradually shift the retention positions of particles/cells in the separation chamber, a density-gradient elution scheme has been proposed. We demonstrated the separation of microparticles with sizes of 1–5  $\mu\text{m}$  and achieved blood cell sorting with this microfluidic CCE system.

## 2 Principle

The principle of a microfluidic CCE is shown in Fig. 1. Unlike a conventional CCE, in which a 3D cone-shaped separation chamber is used, a planar wedge-shaped chamber is employed here. First, the entire microchannel network is filled with a medium of relatively low density. Then a particle suspension with the same fluid density is dropped into the inlet reservoir. Particles are loaded into the separation chamber by generating fluid flow via device rotation instead of pressure-driven pumping devices (Fig. 1a). In the separation chamber, particles are subjected to the centrifugal force in an outward direction and to the fluid force in an inward direction simultaneously, as in a conventional CCE. At a given rotation speed, the centrifugal force near the entrance of the separation chamber is higher than that near the exit, depending on the distance from the center of rotation. The fluid force ( $\sim$ flow rate) near the entrance is also higher than that near the exit, depending on the cross-sectional area of the chamber. Therefore, a particle with a specific sedimentation velocity retains its position at a specific point in the separation chamber depending on particle size, shape, and density, where the centrifugal and fluid forces are balanced (Fig. 1b). Particles with very small sizes and/or low densities do not remain in the chamber and flow through the channel system toward the outlet. Introducing a fluid with a higher density into the microchannel decreases the centrifugal force on the particles without significantly changing the flow rate, resulting in the stepwise elution of particles based on the sedimentation velocity (Fig. 1c).

In order to effectively focus particles into the center of the separation chamber, we employed a branched loading channel as shown in Fig. 1a. At the branch point, fluid flow is almost equally split into two streams and recombined before entering the separation chamber. Particles tend to flow near the outer sidewall in the loading channel because of the centrifugal force, and so particles selectively flow through one of the two branches. As a result, particles are focused to the center of the separation chamber due to the centrifugal force and the presence of particle-free fluid flow.

**Fig. 1** Principle of microfluidic counterflow centrifugal elutriation. **a** Particle introduction by the rotation-driven flow. Particles are focused to the center of the separation chamber by the split flow. **b** Particle retention at certain positions in the separation chamber depending on the particle size and density, where the centrifugal force and fluid drag force are balanced. Very small or low-density particles are not retained in the chamber. **c** Stepwise elution and recovery of particles by introducing a fluid with a higher density



We perform a simple theoretical estimate of these two forces in the separation chamber. The centrifugal force applied to a spherical particle in the rotating chamber,  $F_c$ , is:

$$F_c = \frac{\pi}{6} D_p^3 (\rho_p - \rho_f) r \omega^2, \tag{1}$$

where  $D_p$  is the particle diameter,  $\rho_p$  and  $\rho_f$  are the densities of the particle and the fluid, respectively,  $r$  is the particle position from the center of rotation, and  $\omega$  is the angular velocity of rotation. The fluid drag force on a particle,  $F_d$ , is given by the following equation when  $Re$  is sufficiently small ( $Re < 1$ ) (Kirby 2010):

$$F_d = 3\pi\eta D_p U(r), \tag{2}$$

where  $\eta$  is the fluid viscosity and  $U(r)$  is the (average) flow velocity at a point  $r$  in the separation chamber.  $U(r)$  is determined by the total volumetric flow rate through the channel system,  $Q$ , and the cross-sectional area of the separation chamber at a point  $r$ ,  $S(r)$ , and expressed as follows:

$$U(r) = \frac{Q}{S(r)} = \frac{\Delta P}{S(r)R_{\text{whole}}}, \tag{3}$$

where  $\Delta P$  is the pressure drop across the fluid inside the microchannel generated by the device rotation, and  $R_{\text{whole}}$

is the hydrodynamic resistance of the entire microchannel. The pressure drop  $\Delta P$  is expressed as follows (Ducrée et al. 2007):

$$\Delta P = \rho_f \omega^2 (r_2 - r_1) r_{\text{mean}}, \tag{4}$$

where  $r_1$  and  $r_2$  are the distances from the center of rotation to the inlet and outlet reservoirs, respectively, and  $r_{\text{mean}}$  is the distance between the center of rotation and the mean radial point of the fluid inside the microchannel. The hydrodynamic resistance  $R_{\text{whole}}$  is given by the sum of the hydrodynamic resistances of the rectangular microchannel segments,  $R_{\text{seg}}$ , expressed as follows (White 2006):

$$R_{\text{seg}} = \frac{12\eta L}{l_1^3 l_2} \left[ 1 - \frac{192l_1}{\pi^5 l_2} \sum_{n=1,3,5}^{\infty} \frac{\tanh\left(\frac{n\pi l_2}{2l_1}\right)}{n^5} \right]^{-1}, \tag{5}$$

where  $l_1$  and  $l_2$  are either the width or the depth ( $l_1$  is the larger of these two values), and  $L$  is the length of the microchannel segment. A particle is retained at a certain point  $r$  in the separation chamber, where  $F_c = F_d$ . In Eqs. (1) and (2), both of these forces are proportional to the square of the angular velocity  $\omega$  and are not a function of fluid viscosity  $\eta$ , suggesting that these factors do not affect the retention positions of particles.

### 3 Experimental

#### 3.1 Microchannel fabrication and design

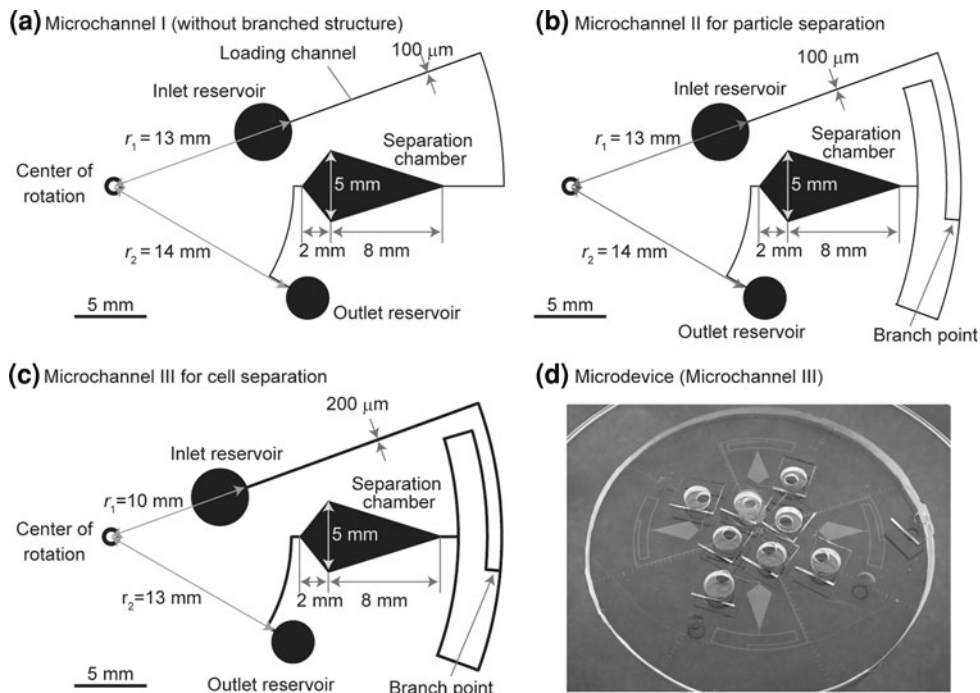
Polydimethylsiloxane (PDMS) microfluidic devices were fabricated using standard soft lithography and replica-molding techniques as described elsewhere (Morijiri et al. 2011). Three types of microchannel designs (Microchannels I, II, and III) and a photograph of a microdevice are shown in Fig. 2. Depths of Microchannels I, II, and III were  $\sim 23 \mu\text{m}$ ,  $\sim 23 \mu\text{m}$ , and  $\sim 27 \mu\text{m}$ , respectively. The diameters of inlet and outlet reservoirs were 2–6 mm and the depth was  $\sim 2 \text{ mm}$ . Each inlet/outlet reservoir was partially covered by a small lid composed of a thin PDMS membrane ( $\sim 500 \mu\text{m}$  in thickness) in order to prevent the fluid from spilling out of the reservoirs during the device rotation.

The wedge-shaped separation chambers were so designed that larger/higher-density particles retain at the narrower region near the entrance, while smaller/lower-density particles retain at the wider region. The width of the widest region of the chamber was 5 mm for all microchannels, where the flow rate is significantly lower than that near the chamber entrance. For example, it was expected that spherical particles larger than  $\sim 2 \mu\text{m}$  would retain in the separation chamber of Microchannels I and II, when the densities of the fluid and particles are 1.00 and  $1.05 \text{ g cm}^{-3}$ , respectively.

#### 3.2 Experimental procedure

In particle separation experiments, fluorescent polystyrene microbeads with a diameter of 1.0, 3.0, or  $5.0 \mu\text{m}$  and density  $\rho_p$  of  $1.05 \text{ g cm}^{-3}$  (B0100 (blue), R0300 (red), or G0500 (green), Duke Scientific Corp., CA, USA) were used. Microbeads were suspended in a 0.5 % (w/v) Tween 80 aqueous solution ( $\rho_f = 1.00 \text{ g cm}^{-3}$ ). In all experiments, the initial concentrations of 1.0, 3.0 and  $5.0\text{-}\mu\text{m}$  particles were  $1.8 \times 10^5$ ,  $2.0 \times 10^4$ , and  $7.0 \times 10^3 \mu\text{L}^{-1}$ , respectively. Before conducting separation experiments, the entire microchannel was hydrophilized by  $\text{O}_2$  plasma, followed by the introduction of the solution without containing particles in order to fill the entire channel. Then the solution in the inlet reservoir was replaced with 5–20  $\mu\text{L}$  of the particle suspension, and the device was rotated on a spinning device (IH-D7, Mikasa Corp., Japan). After a certain period of time, the device rotation was stopped, and the openings of the inlet and/or outlet reservoirs were reversibly sealed by thin PDMS membranes, in order to prevent the flow generation inside the microchannel system during observation. The particle positions were observed using an inverted microscope (IX-71, Olympus Corp., Japan) and a CCD camera (DP72, Olympus). After recovering the particles retained in the outlet reservoir by pipetting, particles were counted by using a hemocytometer. Then a buffer solution with the same or higher density was introduced into the inlet reservoir, and the rotation

**Fig. 2** Microchannel designs. **a** Microchannel I without the branched channel, **b** microchannel II with the branched loading channel used for polymer particle separation, and **c** microchannel III for cell separation. **d** Photograph of the PDMS microdevice incorporating four identical microchannels



operation was repeated. As a high-density buffer solution, we employed aqueous solutions of cesium chloride. The densities of 2.7 and 5.4 % (w/v) CsCl solutions were 1.02 and 1.04 g cm<sup>-3</sup>, respectively.

For blood cell separation, peripheral blood was obtained from a healthy volunteer by using a finger-puncture device. The cell suspension was prepared by diluting 10 μL of whole blood with 490 μL phosphate buffered saline (PBS) containing 0.1 % (w/v) bovine serum albumin. This solution was also used as the buffer solution. Leukocytes were selectively labeled by adding 0.1 mg mL<sup>-1</sup> Hoechst 33342 dye (Invitrogen Corp., CA, USA) into the cell suspension. As a medium of higher density, Lymphoprep ( $\rho_f = 1.077$  g cm<sup>-3</sup>; Cosmo Bio Co. Ltd., Tokyo, Japan) was used in order to elute the retained cells from the chamber.

## 4 Results and discussion

### 4.1 Particle focusing using a branching structure

First, we examined the effect of the branched loading channel on particle focusing in the separation chamber. Particle behaviors in two types of microdevices (Microchannels I and II) were compared using 5.0-μm particles. For Microchannel I, which did not have a branching channel (Fig. 2a), we observed a severe accumulation of particles on the lower sidewall after rotating for 1,200 s at 1,500 rpm (Fig. 3a). The majority of the introduced particles accumulated at ~1 mm from the entrance. This accumulation was caused by the centrifugal alignment of particles to the outer sidewall in the loading channel. The particles did not move further because the centrifugal and fluid forces near the sidewall were not equal and opposite, due to the expanding structure of the separation chamber. This accumulation made it difficult to achieve particle retention at different positions according to size/density.

In order to solve this accumulation problem and fully exploit the effects of the two forces in the separation chamber, a microchannel with a branched loading channel (Microchannel II) was designed and fabricated as shown in Fig. 2b. Since the dimensions (width, depth, and length) of the two branches were equal, the introduced fluid flow would be equally divided into two streams and recombined just before entering the separation chamber. Figure 3b shows the 5.0-μm particles being introduced into the separation chamber after rotating for 900 s at 1,500 rpm. The initial positions of particles near the chamber entrance were almost perfectly focused at the center because of the equally divided and recombined streams and the particle alignment on the outer sidewall just before entering the confluence [Line (3) in Fig. 3b]. We observed that ~90 % of the particles were located between 3 and 6 mm from the

chamber entrance. Particle positions were gradually dispersed after entering the chamber [Lines (1) and (2)], and ~5 % of particles were located on the sidewalls. This dispersion in the width direction can be attributed to particle diffusion caused by the Brownian motion, together with the imbalanced fluid drag and centrifugal forces; when the particle position deviates a little from the centerline of the chamber, this replacement would be enhanced by the centrifugal force applied in an oblique direction. In addition, some particles on the sidewall moved toward the entrance of the chamber because of the significantly lower flow rate present near the sidewalls. However, we confirmed that a simple branching structure greatly improved particle focusing to the center of the separation chamber, which is a prerequisite for conducting stepwise elution of particles. The 5.0 μm polystyrene particles used here flowed on the bottom surface of the microchannel due to gravity, resulting in a relatively narrow distribution of the particle positions despite the presence of a parabolic flow-rate distribution in the depth direction.

### 4.2 Effects of rotation speed and fluid viscosity

Unlike a conventional CCE, the present system does not independently control the fluid and the centrifugal forces, since both are simultaneously generated by the centrifugal rotation of the device. We first examined the effects of the rotation speed on the retention positions of 5.0-μm particles using Microchannel II, which is the most important factor for operation. The rotation speed was changed from 1,000 to 3,000 rpm. Rotation period was also changed depending on the rotation speed, because volumetric flow rate is proportional to the square of the rotation speed. Initially, the particle suspension was introduced into the inlet reservoir and the device was rotated for 300, 100, and 100 s for rotation speeds of 1,000, 2,000, and 3,000 rpm, respectively. Then, 0.5 % (w/v) Tween 80 aqueous solution was introduced, and the device was rotated for 2,100, 600, and 300 s for the same sequence of rotation speeds.

The results are shown in Fig. 4a. Although the flow rates for 2,000 and 3,000 rpm were expected to be four and nine times faster than that for 1,000 rpm, respectively, ~85 % of the introduced particles in the chamber were retained between 3.5 and 5.5 mm from the entrance of the chamber for all conditions after rotation. The average retention positions ± standard deviation (SD) of particles from the chamber entrance were 4.8 ± 0.5, 4.1 ± 0.8, and 4.1 ± 0.9 mm, for rotation speeds of 1,000, 2,000, and 3,000 rpm, respectively. Therefore, retention positions were not significantly affected by the rotation speed (Fig. 4a), consistent with the theoretical estimate above that the increase in angular velocity increases both centrifugal and fluid forces, which cancel each other. Thus, accurate control of rotation speed is

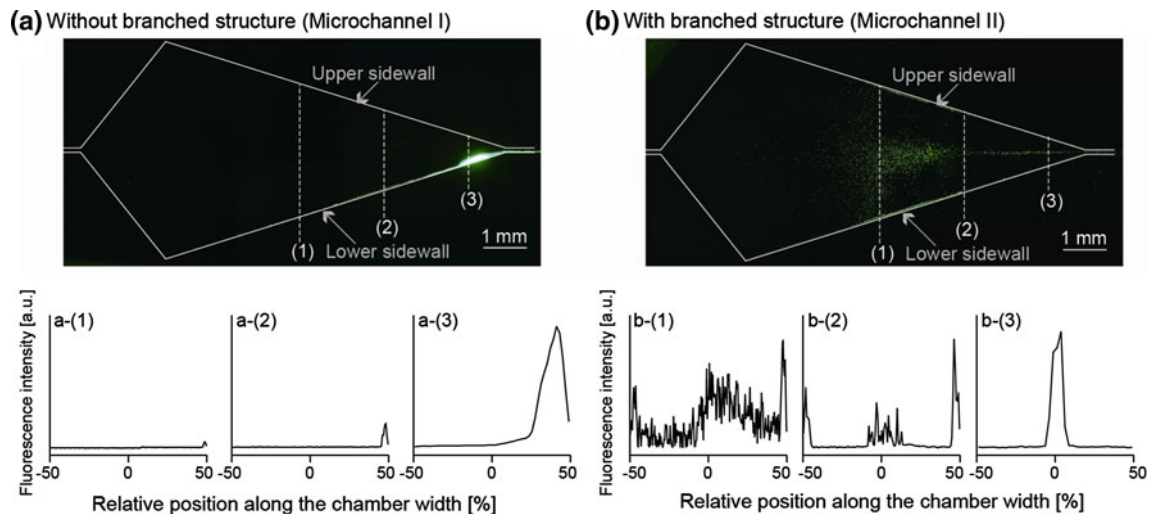


**Fig. 3** Fluorescence micrographs of 5- $\mu\text{m}$  green fluorescent particles loaded into the separation chamber, with the corresponding fluorescence intensity profiles along the dotted lines (1)–(3). Microchannels I (a) and II (b) were used and device rotation was stopped after 900 s at

1,500 rpm. The lines (1), (2), and (3) are located 5, 3, and 1 mm from the chamber entrance, respectively. In each graph,  $-50$ ,  $0$ , and  $50$  % positions correspond to the upper sidewall, center of the chamber, and the lower sidewall, respectively

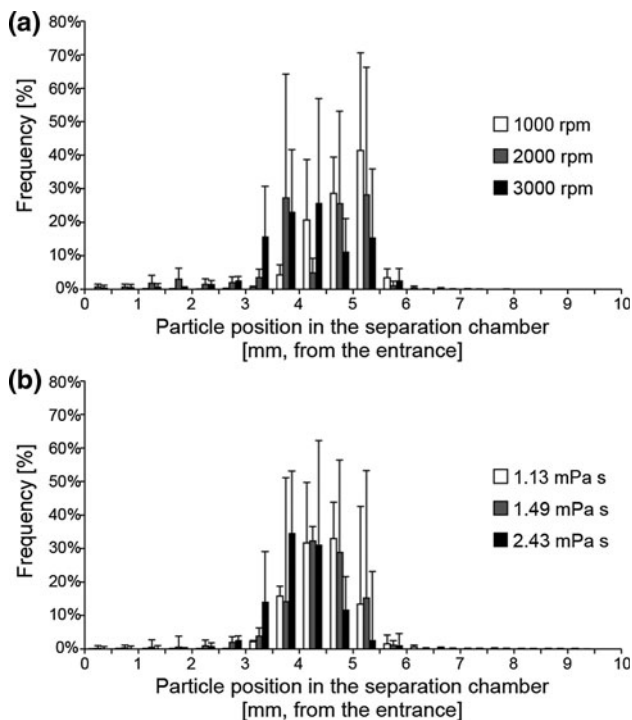


**Fig. 4** Effect of **a** the rotation speed and **b** fluid viscosity on the retention positions of 5.0- $\mu\text{m}$  polystyrene particles in the separation chamber. In **a** 0.5 % Tween 80 aqueous solution was used with a viscosity of 0.94 mPa s. In **b** the microdevice was rotated for 300–900 s at 2,000 rpm

not necessary for particle retention and separation, unless the flow rate becomes extremely high or low.

Next, we examined the effect of fluid viscosity on particle retention. Viscosity changes with temperature, and so a cell-sorting system unaffected by viscosity is highly

versatile and beneficial for wider applications. We changed the viscosity of the medium to 1.13, 1.49, and 2.43 mPa s by adding 2.0 % (w/v) polyethylene glycol (PEG) with different molecular weights of 1,000, 6,000, and 35,000, respectively. The particle suspension was introduced at a rotation speed of 2,000 rpm. The same buffer without containing particles was subsequently introduced at the same rotation speed. As a result,  $\sim 88$  % of the particles were retained in the chamber region between 3.5 and 5.5 mm from the entrance, as shown in Fig. 4b. The positions of the particles from the chamber entrance (mean  $\pm$  SD) were  $4.5 \pm 0.7$ ,  $4.4 \pm 0.7$ , and  $4.1 \pm 0.7$  mm, for viscosities of 1.13, 1.49, and 2.43 mPa s, respectively. Therefore, fluid viscosity did not have a significant effect on the separation of particles. This result is also consistent with our theory that both the centrifugal and the fluid forces are independent of the viscosity, showing the robustness of the present system against the operation conditions such as temperature.

#### 4.3 Separation of particle mixture

We demonstrated the separation and individual recovery of a particle mixture of three different sizes. Since the retention positions of particles were not affected by the rotation speed and fluid viscosity, we employed a density gradient to shift the balance of the centrifugal and fluid forces. From the theoretical estimate given previously, an increase in the fluid density reduces the centrifugal force  $F_c$ , but does not affect the fluid drag force  $F_d$ , achieving a stepwise elution of particles. We used aqueous solutions of CsCl as a high-density fluid, which is generally used for

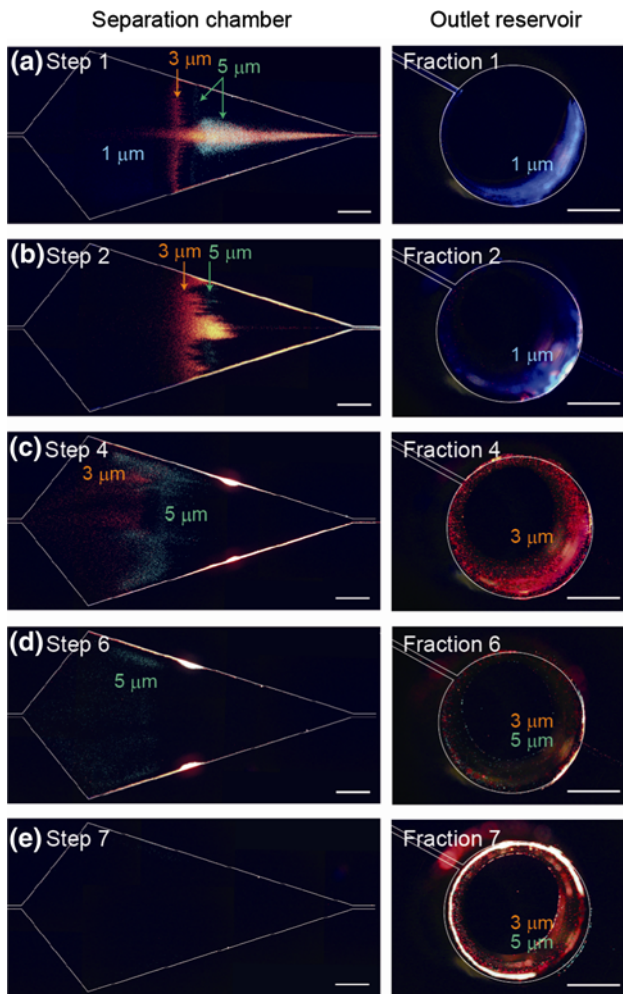


**Fig. 5** Fluorescence micrographs of the separation chamber and the outlet reservoir after each rotation step. **a, b** Particle introduction with a low-density fluid ( $\rho_f = 1.00 \text{ g cm}^{-3}$ ). Small particles (1.0  $\mu\text{m}$ , blue) flowed through the separation chamber. **c, d** Selective elution of 3.0- $\mu\text{m}$  red particles by introducing a fluid with a higher density ( $\rho_f = 1.02 \text{ g cm}^{-3}$ ). **e** Elution of 5.0- $\mu\text{m}$  particles by using the fluid with a density of  $1.04 \text{ g cm}^{-3}$ . Scale bar 1 mm. The channel/chamber walls are outlined by white lines

density-gradient centrifugation. Microchannel II was rotated at 1,500 rpm for this experiment.

The retention and elution behaviors of particles are shown in Fig. 5, and the particle recovery results are shown in Fig. 6. During the first rotation for 300 s, 1.0- $\mu\text{m}$  particles flowed through the channel system to the outlet because the centrifugal force on these small 1.0- $\mu\text{m}$  particles was too low. On the other hand, 3.0 and 5.0- $\mu\text{m}$  particles were retained in the separation chamber (Fig. 5a). After introducing a low-density buffer solution into the channel system 3 times, almost all of the 1.0- $\mu\text{m}$  particles were recovered from the outlet, whereas 3.0 and 5.0- $\mu\text{m}$  particles were retained in the chamber at  $\sim 5.3$  and  $\sim 4.4$  mm from the entrance, respectively (Fig. 5b). After introducing a

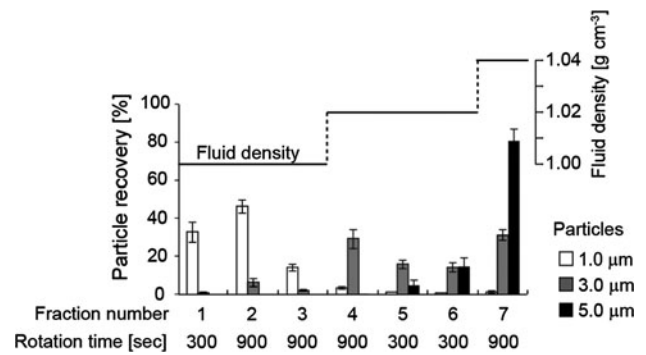


**Fig. 6** Result for particle separation. Particles in each fraction were recovered from the outlet reservoir and counted with a counting chamber. Each data set shows the mean  $\pm$  SD from at least three independent experiments

higher-density buffer [ $\rho_f = 1.02 \text{ g cm}^{-3}$ ; 2.7 % (w/v) CsCl and 0.5 % (w/v) Tween 80 aqueous solution], particle positions shifted inward, and we achieved the selective elution of the 3.0- $\mu\text{m}$  particles (Fig. 5c, d). The remaining 5.0- $\mu\text{m}$  particles were finally eluted from the chamber by increasing the fluid density to  $1.04 \text{ g cm}^{-3}$  [5.4 % (w/v) CsCl and 0.5 % (w/v) Tween 80 aqueous solution], resulting in the separation of microparticles according to size (Fig. 5e). As shown in Fig. 6, we successfully demonstrated the separation of 1.0, 3.0, and 5.0- $\mu\text{m}$  particles by simply changing the fluid density stepwise. The ratio of the 3.0- $\mu\text{m}$  particles in Fraction 7 was  $\sim 30$  %, which was due to the elution of the accumulated 3.0- $\mu\text{m}$  particles on the sidewalls as observed in Fig. 5c, d. Although this demonstration took a relatively long period of time for fluid transportation and particle recovery, the required time could be further shortened by increasing the rotation speed, which does not significantly affect the separation efficiencies. Also, we manually introduced fluids with different densities and manually recovered the output samples, but a further improvement would be possible in terms of integrating multiple inlet/outlet structures for automated introduction and recovery of fluids.

#### 4.4 Blood cell separation

In order to confirm the applicability of the present system for cells, we separated erythrocytes and leukocytes from a diluted blood sample. Since the blood cells (especially leukocytes) are larger than the particles used above, we employed Microdevice III with a broader microchannel (200  $\mu\text{m}$  in width and 27  $\mu\text{m}$  in depth). The increase in the channel width decreases the hydrodynamic resistance of the entire microchannel network, resulting in a higher flow rate in the separation chamber, which makes it easier to balance the centrifugal and fluid forces for relatively large and high-density particles/cells. The density of erythrocytes

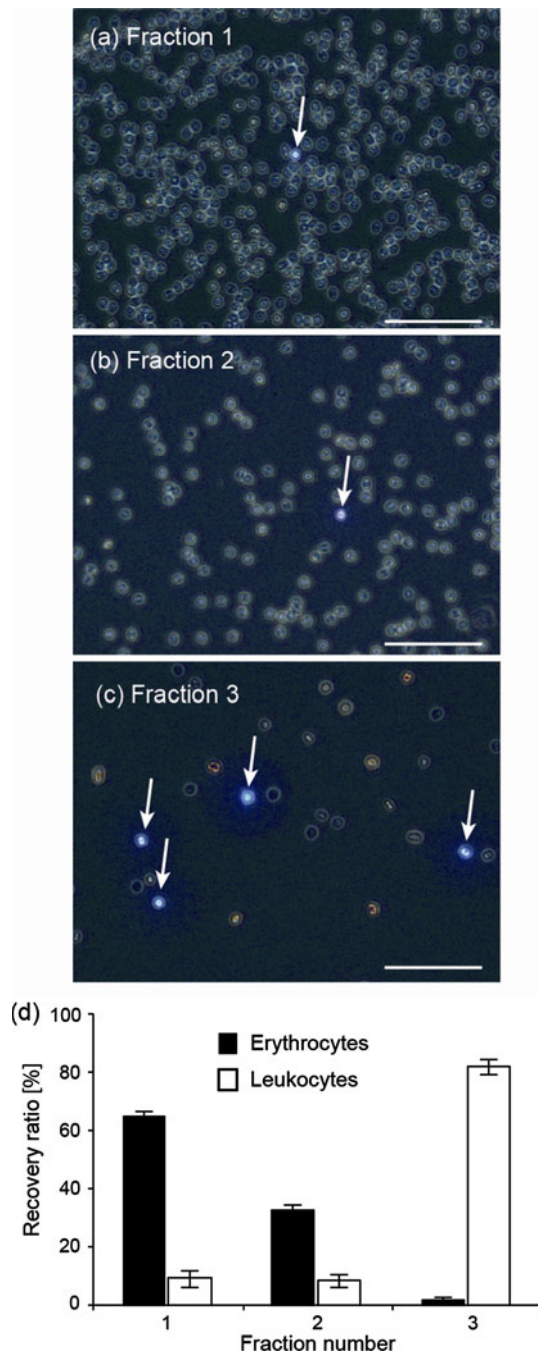


**Fig. 7** **a–c** Micrographs of blood cells in each fraction. Leukocytes are stained in blue by Hoechst 33342 and indicated by *white arrows*. *Scale bar* 100  $\mu\text{m}$ . **d** Recovery ratios of erythrocytes and leukocytes in each fraction. Each data shows the mean  $\pm$  SD of three independent experiments

( $\sim 1.10 \text{ g cm}^{-3}$ ) is higher than that of leukocytes ( $1.062\text{--}1.082 \text{ g cm}^{-3}$ ), but the leukocytes ( $5\text{--}20 \mu\text{m}$ ) are larger than the disk-shaped erythrocytes (diameter  $\sim 7 \mu\text{m}$ , thickness  $\sim 2 \mu\text{m}$ ) (Petersson et al. 2007).

The results of blood cell separation are shown in Fig. 7. During the first rotation at 2,000 rpm for 720 s following

the introduction of 20  $\mu\text{L}$  of the diluted blood sample with a medium density of  $1.00 \text{ g cm}^{-3}$ , most of the loaded erythrocytes were eluted through the separation chamber (Fraction 1, Fig. 7a), whereas most leukocytes were retained. By introducing 20  $\mu\text{L}$  of the buffer and rotating for 900 s, the remaining erythrocytes were washed out of the chamber (Fraction 2, Fig. 7b). At this stage,  $\sim 98 \%$  of erythrocytes were recovered from the outlet, whereas  $\sim 80 \%$  of leukocytes were still retained in the chamber. Assuming an initial hematocrit value of 50 %, the total volume of the introduced cells was  $\sim 0.2 \mu\text{L}$ , a high value comparable to the volume of the separation chamber ( $0.54 \mu\text{L}$ ). However, the selective retention of leukocytes was possible because most of the erythrocytes flowed through the separation chamber. Finally, the introduction of 20  $\mu\text{L}$  of the higher-density buffer (Lymphoprep:  $\rho_f = 1.08 \text{ g cm}^{-3}$ ) achieved the complete elution and recovery of leukocytes (Fraction 3, Fig. 7c). After the introduction of this high-density medium, no cells were observed in the chamber. The ratio of leukocytes in the initial sample was  $\sim 1/1,000$  of that for erythrocytes, but  $\sim 1/20$  of that for Fraction 3, showing the significant enrichment of leukocytes. These results show that the present microdevice mainly utilizes the size rather than the density of the blood cells for their separation, because the mass of an erythrocyte ( $\sim 8 \times 10^{-11} \text{ g}$ ) is significantly lower than that of a leukocyte ( $\sim 5 \times 10^{-10} \text{ g}$  for  $10\text{-}\mu\text{m}$ -size leukocyte). Small leukocytes with a size of  $\sim 5 \mu\text{m}$  have a mass comparable to that of erythrocytes, which could be eluted from the chamber together with the erythrocytes. In this study, we just demonstrated the separation of leukocytes and erythrocytes into several fractions. However, a future study would include the separation of leukocytes into multiple fractions, such as the separation of granulocytes and lymphocytes with different densities.

## 5 Conclusions

We developed a centrifugal microfluidic device for the precise separation of particles/cells, which utilizes both the centrifugal and fluid forces generated by device rotation. A density-gradient elution scheme was proposed in order to achieve the efficient and stepwise elution of particles. In addition, the branched microchannel geometry greatly improved the focusing and introduction of particles to the center of the separation chamber. Compact PDMS devices are inexpensive and suitable for disposable use, and the simple and robust separation mechanism is useful for clinical and research applications. Although several improvements should be made in terms of increasing the throughput and developing automated introduction and recovery systems of fluid samples, the present system



would be particularly effective for separating a small amount of precious samples or purifying rare cells from a complex mixture.

**Acknowledgments** This research was supported in part by Grants-in-aid for Scientific Research A (20241031) and Priority Areas (23106007) from Ministry of Education, Culture, Sports, Science, and Technology (MEXT), Japan, and for Improvement of Research Environment for Young Researchers from Japan Science and Technology Agency (JST).

## References

- Bauer J (1999) Advances in cell separation: recent developments in counterflow centrifugal elutriation and continuous flow cell separation. *J Chromatogr B Biomed Sci Appl* 722(1–2):55–69
- Brenner T, Glatzel T, Zengerle R, Ducree J (2005) Frequency-dependent transversal flow control in centrifugal microfluidics. *Lab Chip* 5(2):146–150
- Cho Y-K, Lee J-G, Park J-M, Lee B-S, Lee Y, Ko C (2007) One-step pathogen specific DNA extraction from whole blood on a centrifugal microfluidic device. *Lab Chip* 7(5):565–573
- Davis JA, Inglis DW, Morton KJ, Lawrence DA, Huang LR, Chou SY, Sturm JC, Austin RH (2006) Deterministic hydrodynamics: taking blood apart. *Proc Natl Acad Sci USA* 103(40):14779–14784
- Donaldson KL, Andrew M, Wahl AF (1997) Separation by counterflow centrifugal elutriation and analysis of T- and B-lymphocytic cell lines in progressive stages of cell division cycle. *J Immunol Methods* 203:25–33
- Ducrée J, Haerberle S, Lutz S, Pausch S, Stetten Fv, Zengerle R (2007) The centrifugal microfluidic bio-disk platform. *J Micromech Microeng* 17(7):S103–S115
- Duffy DC, Gillis HL, Lin J, Sheppard NF Jr, Kellogg GJ (1999) Microfabricated centrifugal microfluidic systems: characterization and multiple enzymatic assays. *Anal Chem* 71:4669–4678
- Faradji A, Bohbot A, Schmitt-Goguel M, Siffert JC, Dumont S, Wiesel ML YP, Eischen A, Bergerat JP, Bartholeyns J, Poindron P, Witz JP, Oberling F (1994) Large scale isolation of human blood monocytes by continuous flow centrifugation leukapheresis and counterflow centrifugation elutriation for adoptive cellular immunotherapy in cancer patients. *J Immunol Methods* 174:297–309
- Gibbs BF, Papenfuss K, Falcone FH (2008) A rapid two-step procedure for the purification of human peripheral blood basophils to near homogeneity. *Clin Exp Allergy* 38(3):480–485
- Gorkin R, Park J, Siegrist J, Amasia M, Lee BS, Park J-M, Kim J, Kim H, Madou M, Cho Y-K (2010) Centrifugal microfluidics for biomedical applications. *Lab Chip* 10(14):1758–1773
- Gorkin R, Soroori S, Southard W, Clime L, Veres T, Kido H, Kulinsky L, Madou M (2012) Suction-enhanced siphon valves for centrifugal microfluidic platforms. *Microfluid Nanofluid* 12(1–4):345–354
- Grumann M, Geipel A, Riegger L, Zengerle R, Ducrée J (2005) Batch-mode mixing on centrifugal microfluidic platforms. *Lab Chip* 5(5):560–565
- Haerberle S, Brenner T, Zengerle R, Ducree J (2006) Centrifugal extraction of plasma from whole blood on a rotating disk. *Lab Chip* 6(6):776–781
- Hou HW, Bhagat AA, Chong AG, Mao P, Tan KS, Han J, Lim CT (2010) Deformability based cell margination—a simple microfluidic design for malaria-infected erythrocyte separation. *Lab Chip* 10(19):2605–2613
- Huh D, Bahng JH, Ling Y, Wei HH, Kripfgans OD, Fowlkes JB, Grotberg JB, Takayama S (2007) Gravity-driven microfluidic particle sorting device with hydrodynamic separation amplification. *Anal Chem* 79(4):1369–1376
- Kim J, Kido H, Rangel RH, Madou MJ (2008) Passive flow switching valves on a centrifugal microfluidic platform. *Sens Actuators B Chem* 128(2):613–621
- Kirby BJ (2010) Micro- and nanoscale fluid mechanics: transport in microfluidic devices, Chapter 8. Cambridge University Press, London
- Lee BS, Lee JN, Park JM, Lee JG, Kim S, Cho YK, Ko C (2009) A fully automated immunoassay from whole blood on a disc. *Lab Chip* 9(11):1548–1555
- Morijiri T, Sunahiro S, Senaha M, Yamada M, Seki M (2011) Sedimentation pinched-flow fractionation for size- and density-based particle sorting in microchannels. *Microfluid Nanofluid* 11(1):105–110
- Nagrath S, Sequist LV, Maheswaran S, Bell DW, Irimia D, Utkus L, Smith MR, Kwak EL, Digumarthy S, Muzikansky A, Ryan P, Balis UJ, Tompkins RG, Haber DA, Toner M (2007) Isolation of rare circulating tumour cells in cancer patients by microchip technology. *Nature* 450(7173):1235–1239
- Overturf K, Al-Dhalimy M, Finegold M, Grompe M (1999) The repopulation potential of hepatocyte populations differing in size and prior mitotic expansion. *Am J Pathol* 155(6):2135–2143
- Pamme N (2007) Continuous flow separations in microfluidic devices. *Lab Chip* 7(12):1644–1659
- Petersson F, Aberg L, Sward-Nilsson AM, Laurell T (2007) Free flow acoustophoresis: microfluidic-based mode of particle and cell separation. *Anal Chem* 79(14):5117–5123
- Siegrist J, Gorkin R, Bastien M, Stewart G, Peytavi R, Kido H, Bergeron M, Madou M (2010) Validation of a centrifugal microfluidic sample lysis and homogenization platform for nucleic acid extraction with clinical samples. *Lab Chip* 10(3):363–371
- Steigert J, Grumann M, Brenner T, Riegger L, Harter J, Zengerle R, Ducree J (2006) Fully integrated whole blood testing by real-time absorption measurement on a centrifugal platform. *Lab Chip* 6(8):1040–1044
- Sugaya S, Yamada M, Seki M (2011) Observation of nonspherical particle behaviors for continuous shape-based separation using hydrodynamic filtration. *Biomicrofluidics* 5(2):024103
- Uchida N, Weissman IL (1992) Searching for hematopoietic stem cells: evidence that Thy-1.1<sup>+</sup> Lin<sup>-</sup> Sea-1<sup>+</sup> cells are the only stem cells in C57BL/Ka-Thy-1.1 bone marrow. *J Exp Med* 175:175–184
- Wahl LM, Katona IM, Wilder RL, Winter CC, Haraoui B, Scher I, Wahl SM (1984) Isolation of human mononuclear cell subsets by counterflow centrifugal elutriation (CCE). I. Characterization of B-lymphocyte-, T-lymphocyte-, and monocyte-enriched fractions by flow cytometric analysis. *Cell Immunol* 85(2):373–383
- White FM (2006) In viscous fluid flow, Chapter 3, 3rd edn. McGraw-Hill Companies, Inc., Boston
- Yamada M, Seki M (2005) Hydrodynamic filtration for on-chip particle concentration and classification utilizing microfluidics. *Lab Chip* 5(11):1233–1239